batteries

Article

Manganese-Coordinated Cellulose Based-Separator for Efficient and Reliable Zn-Ion Transport

Jiazhe Cheng [1], Kai Wang [1,2], Xiaoyu Ning [3], Jichao Zhang [1], Hao Jia [1,2,*], Benjamin Tawiah [4,5,*] and Shouxiang Jiang [4,6,*]

1 National Manufacturing Innovation Center of Advanced Dyeing and Finishing Technology, Jiangnan University, Wuxi 214122, China; 1092220217@stu.jiangnan.edu.cn (J.C.); 6233014012@stu.jiangnan.edu.cn (K.W.); jichaozhang@jiangnan.edu.cn (J.Z.)
2 College of Textile & Garment, Shaoxing University, Shaoxing 312000, China
3 Shanghai Institute of Space Power-Sources, Shanghai 200245, China; 242592891@st.usst.edu.cn
4 School of Fashion and Textiles, The Hong Kong Polytechnic University, Hong Kong, China
5 Department of Industrial Art (Textiles), Kwame Nkrumah University of Science and Technology, Kumasi AK-417-4732, Ghana
6 Research Centre of Textiles for Future Fashion, The Hong Kong Polytechnic University, Hong Kong, China
* Correspondence: jiahao@jiangnan.edu.cn (H.J.); benjamin.tawiah@connect.polyu.edu.hk (B.T.); kinor.j@polyu.edu.hk (S.J.)

Abstract: Aqueous zinc-ion batteries (AZIBs) are increasingly being acknowledged as a promising candidate to safely power large-scale energy storage systems and portable devices. However, the development of effective separator materials remains a significant challenge due to issues such as harmful dendrite growth on zinc (Zn) anodes and parasitic side reactions in aqueous electrolytes. To address this challenge, we synthesize a manganese-coordinated cellulose nanofibril (Mn-CNF)-based separator for high-performance AZIBs. This separator affords enhanced ion transport channel, a large number of hydroxyl groups, and exceptional mechanical properties, with a tensile strength of 2.8 MPa and superior ionic conductivity of 5.14 $mS \cdot cm^{-1}$. These attributes collectively enhance Zn-ion transport, minimize nucleation overpotential for Zn, and accelerate the Zn deposition kinetics, thus significantly outperforming the untreated CNF separators. Consequently, the Zn||MnO_2 battery with the Mn-CNF separator shows a marked improvement in the galvanostatic rate performance and cycling stability by effectively accelerating and optimizing Zn-ion transport. This study offers valuable insights into the development of efficient and reliable separators for advanced electrochemical energy storage technologies.

Keywords: aqueous zinc-ion batteries; cellulose nanofibril; functional separator; facilitated ion transport; Zn dendrites

Citation: Cheng, J.; Wang, K.; Ning, X.; Zhang, J.; Jia, H.; Tawiah, B.; Jiang, S. Manganese-Coordinated Cellulose Based-Separator for Efficient and Reliable Zn-Ion Transport. *Batteries* **2024**, *10*, 416. https://doi.org/10.3390/batteries10120416

Received: 27 October 2024
Revised: 21 November 2024
Accepted: 25 November 2024
Published: 27 November 2024

1. Introduction

Lithium-ion batteries (LIBs) are the most commonly used energy storage systems for powering mobile electronics and electric vehicles because they have an exceptional electrochemical performance [1,2]. However, the high demand for lithium with the widespread use of large-scale electronic devices and portable gadgets could cause its shortage and mining lithium also requires time [3,4]. Thus, there is a need to explore other high-performing electrochemical energy storage options to supplement LIBs and meet the increasing need for energy storage in different contexts [5,6]. Among the emerging alternatives, aqueous zinc-ion batteries (AZIBs) have been touted as a potential candidate because they are very safe to use, there is an abundance of raw materials used to produce them, and they are cost-efficient [7]. Unlike LIBs, AZIBs use aqueous electrolytes which do not require a dry environment during the manufacturing process so there are no added costs to designing and operating a dry room. AZIBs also enhance ionic conductivity which improves their overall

performance [8]. This environmentally sustainable option should be the best candidate to meet the demands for flexible energy storage devices that can be seamlessly integrated with wearable technology. Nevertheless, the zinc (Zn) anodes in AZIBs are susceptible to dendrite formation due to irregular electric fields and the accumulation of charge on the Zn tips, thus increasing parasitic reactions, by-product accumulation, and electrode impedance [9,10]. The proliferation of dendrites can perforate separators, thus resulting in short circuits, rapid capacity degradation, and impaired cycling stability. As such, AZIBs are not often used for practical applications.

In battery configurations, separators play a crucial role in the different electrochemical functions and ensure operational safety [11,12]. However, the current use of glass fiber-based separators is not only expensive but also has several limitations which include irregular and large pore sizes that prevent the selective regulation of ion transport in the electrolyte, leading to the irregular flux of Zn ions and increasing dendrite growth on the surface of the Zn anode.

Cellulose, a fundamental structural component of wood and plant cell walls, is widely recognized as one of the most abundant natural materials on Earth [13,14]. Cellulose is a sustainable material with versatile properties; therefore it is a promising candidate for applications in ionic devices [15]. Cellulose can form organized fibers and nanofibers and has one-dimensional molecular chains. Utilizing cellulose nanofibers, which are structured from primary fibers approximately 2 nanometers in size, creates smaller ion transport pathways at an ultra-microscopic angstrom scale, thus providing a compelling approach for engineering applications [16]. Through the targeted manipulation of the linear molecular chains of cellulose which are composed of polysaccharides with numerous interconnected anhydroglucose units (AGUs), the properties of cellulose can be tailored for different scientific and industrial applications [17]. Each cellulose disaccharide unit contains two primary and four secondary alcohol groups, which result in cellulose colloids that are very hydrophilic and swell when exposed to water. The linear configuration and swelling properties of cellulose facilitate the formation of intricately entangled three-dimensional network structures that promote rapid and selective ion transport [18].

Recent progress in the development of cellulose-based separators for AZIBs has been remarkable [19,20]. These innovative separators play a crucial role in enhancing the performance and efficiency of such batteries. For example, Huang et al. designed a composite separator consisting of ceramics and cellulose [21]. This material is intended to facilitate uniform Zn deposition, improve the movement of Zn^{2+} ions, and repel anions. These characteristics jointly contribute to the stabilization of the zinc anode and effectively prevent passivation reactions that could hamper battery performance. Additionally, Qin et al. fabricated a tungsten carbide (WC)–cellulose nanofiber (WCCNF) composite separator by using a straightforward solution-casting method [22]. The WCCNF separator is particularly efficient in achieving a dendrite-free zinc anode, a feature that is essential for battery safety and durability. Nevertheless, there is a significant demand for the development of high-performance cellulose-based separators that can be produced through more cost-efficient and simplified manufacturing processes.

In this study, we investigate a novel engineering approach which increases the intermolecular polymer structure and improves Zn^{2+} transport kinetics with exceptionally high ionic conductivity. We explore this approach by using cellulose nanofibrils (CNFs), which have an aligned hierarchical structure that is usually found in oxygen-containing polar functional groups (e.g., hydroxyl) within repeating AGUs that constitute the cellulose molecular chains. These polar functionalities are capable of solvating Zn^{2+} ions, thus facilitating their rapid movement. Through the Mn^{2+} coordination of the CNF-based separator (Mn-CNF) via a scalable solvent exchange process, we demonstrate the increase in spacing between polymer chains to create molecular channels, which enables the acceleration of Zn^{2+} transport. Within these designed conduction passages, the functional groups of cellulose, which have an abundance of oxygen, along with the bound water, contribute to Zn^{2+} movement independently of polymeric segmental relaxation.

2. Materials and Methods

2.1. Materials

Sodium hydroxide and manganous sulfate were purchased from Sinopharm Chemical Reagent Co., Ltd., Shanghai, China. CNF membranes were purchased from Taizhou Aoke Filter Paper Factory (201), Taizhou, China.

2.2. Preparation of Mn-CNF Separator

To prepare the Mn-CNFs, a 20 wt.% solution of sodium hydroxide was prepared by dissolving 10 g of sodium hydroxide in 40 g of deionized water. The solution was magnetically stirred until a homogeneous solution was obtained. After the solution cooled down, 0.68 g of manganous sulfate in the powder form was gradually added to the solution. The mixture was again magnetically stirred at 25 °C until the transparent colorless solution became a translucent flesh color. Subsequently, the CNF was immersed in this solution for 24 h. Afterwards, the CNF was removed, thoroughly washed with deionized water, and vacuum-dried at 60 °C for 9 h to produce the Mn-CNF separator.

2.3. Material Characterization

The phase composition of the separators was investigated by using X-ray diffraction (XRD) with a D8 Advance instrument (Bruker, Billerica, MA, USA) and a Cu Kα radiation source (λ = 1.5406 Å), which was operated at 40.0 kV and 40.0 mA, respectively. Scanning electron microscopy (SEM) imaging and energy-dispersive X-ray spectroscopy analyses were performed with an FEI Tecnai G2 F20 transmission electron microscope (Hitachi, Tokyo, Japan). The Raman spectra were recorded by using a LabRam HR-800 spectrometer (Renishaw, London, UK) with a laser wavelength of 514 nm. The contact angles of a 100 μL electrolyte droplet on the Zn foil were measured with a contact angle goniometer (JC2000DM, Zhongchen Co., Ltd., Suzhou, China). The microstructural features of the surface of the Zn electrode were examined with an ultra-depth three-dimensional microscope (VHX-1000C, Keyence, Osaka, Japan). Fourier transform infrared spectroscopy (FTIR) was conducted by using a Nicolet iS50 FTIR microspectrometer (Thermofisher, Waltham, MA, USA). The tensile properties of Mn-CNF separators were evaluated by Daojin EZ-LC universal testing machine (Tokyo, Japan).

2.4. Electrochemical Measurements

Electrochemical characterization was conducted by using CR2032 coin cells (Tianjin EVS Chemical Technology Co., Ltd., Tianjin, China) with 2 M $ZnSO_4$ under standard conditions. To determine the durability of the Zn foil anodes (Tianjin EVS Chemical Technology Co., Ltd.) with a thickness of 0.1 mm, symmetric Zn||Zn configurations were used for the extended galvanostatic cycling tests. Electrochemical impedance spectroscopy (EIS) measurement frequency ranged from 0.1 Hz to 1 MHz and cyclic voltammetric (CV) curves were tested on a VersaSTAT 3F workstation. The Coulombic efficiency (CE) of the Zn deposition and dissolution processes was determined at a potential threshold of 0.5 V versus Zn/Zn^{2+} on carbon cloth (CC, plain weave fabric, China Phychemi Co., Ltd., Hong Kong, China) with a thickness of 0.5 mm, as a working electrode. To fabricate the conductivity test cells, stainless steel electrodes (Tianjin EVS chemical technology Co., Ltd.), with thicknesses of 0.01 mm, were separated by using a standard separator in a coin cell housing.

For the assembly of the Zn||MnO_2 batteries, MnO_2 was prepared following established protocols [23]. This was then combined with acetylene black (Tianjin EVS Chemical Technology Co., Ltd.) and polyvinylidene fluoride (PVDF, Arkema Co., Ltd., Colombes, France) at a weight ratio of 7:2:1, with N-methylpyrrolidone (NMP, Aladdin Co., Ltd., Shanghai, China) serving as the dispersion medium. The composite was uniformly coated onto titanium foil substrates (0.01 mm in thickness, Tianjin EVS Chemical Technology Co., Ltd.) to achieve a final electrode with a thickness of around 0.02 mm. Comprehensive electrochemical assessments were performed by using a CHI660e workstation, AMETEK

Versa STAT 3F, and LAND CT3001A battery tester. The calculated specific capacities for the full batteries were normalized to the mass of the MnO_2 cathode material.

3. Results and Discussion

Mn-CNF separators were prepared by using a simple immersion process from the natural wood resources as shown in Figure 1a; the substrates were immersed into an alkaline Mn ion solution and induced the formation of ionic coordination structures between Mn ion and cellulose chains. Figure 1b shows the cellulose separator before and after the Mn coordination treatment. After the coordination treatment with the Mn ion solution, the cellulose separator changes from a white to darker pink color. The color is also more uniform, thus indicating that Mn-CNFs have effectively incorporated the Mn ions. To further characterize the Mn-coordinated separator, SEM and EDS tests were conducted on the Mn-CNFs. Figure 1c shows the SEM image of an Mn-CNF and the distribution of C, O, and Mn on the sample. The elemental mapping images show that Mn is uniformly dispersed on the separator and accounting 17.5% weight percentage of the total separator (Table 1).

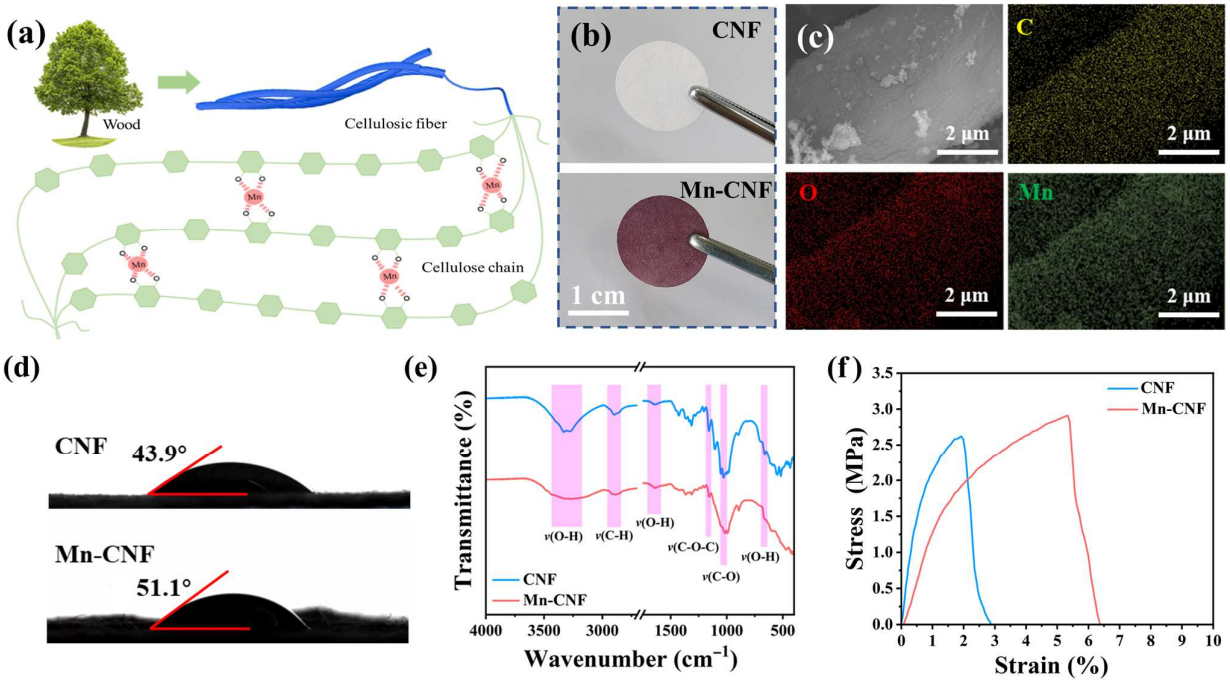

Figure 1. (**a**) Schematic of the fabrication process of Mn-CNF separator, (**b**) digital photos of CNF and Mn-CNF, (**c**) SEM images with EDS mapping of Mn-CNF, (**d**) contact angles, (**e**) FTIR spectra, and (**f**) stress–strain curves of CNF vs. Mn-CNF.

Table 1. Weight percentage of different elements in Mn-CNF separator.

Element	Weight (%)
C	52.4
O	30.1
Mn	17.5

To investigate whether Mn coordination affects the wettability of a cellulose separator and its feasibility as a separator for AZIBs, contact angle tests with a Zn sulfate solution were performed on both Mn-CNFs and CNFs. As shown in Figure 1d, the contact angle of the CNF is 43.9°, while that of the Mn-CNF is slightly larger at 51.1°, thus indicating that the wettability of the CNF-based separator to the Zn sulfate electrolyte is somewhat reduced after Mn coordination [24]. However, a contact angle smaller than 90° is generally considered wettable, so the Mn-CNF is still considered to exhibit good wettability.

Additionally, infrared spectroscopy and Zeta potential tests were conducted on the CNFs and Mn-CNFs to explore the impact of Mn coordination on their internal structure and the surface charge of the cellulose fibers. Figure 1e presents the results of the infrared spectroscopy tests for Mn-CNF and CNF. Both samples show a strong OH- vibration peak at 3300 cm^{-1}, thus indicating that they both have good hydrophilicity [25]. The absorption intensity of Mn-CNF at this vibration peak is slightly lower than that of CNF, which is in agreement with the contact angle results and further explains the difference in wettability to the electrolyte between the CNFs and Mn-CNFs. As illustrated in Figure S1, the large number of hydroxyl functional groups in the cellulose contributes to high electronegativity, which results in a Zeta potential of −35.35 mV for the CNFs. The coordination of the Mn^{2+} ions in the cellulose structure leads to a reduction in the surface electronegativity, thus causing the Zeta potential of the Mn-CNFs to increase to −25.43 mV. Moreover, AZIB separators need to have good mechanical properties. High strength effectively limits the growth of Zn dendrites, whereas poor mechanical properties render Mn-CNFs vulnerable to penetration by the Zn dendrites. As shown in Figure 1f, the Mn-CNF shows a higher tensile strength of 2.85 MPa compared to the CNF which has a tensile strength of 2.61 MPa.

Ionic conductivity is another critical parameter of separators, which directly influences the power density of batteries [26]. As shown in Figure 2a, EIS is used to measure the stainless steel (SS)||SS battery with CNFs and Mn-CNFs as the separator. The ionic conductivity of the electrolyte-soaked Mn-CNFs is 5.148 $mS{\cdot}cm^{-1}$, which is higher than that of the CNFs (0.507 $mS{\cdot}cm^{-1}$). Figure 2b shows the CE of the Zn||CC cells, which use both Mn-CNFs and CNFs. The former shows a slightly higher average CE of 98.19%, compared to 96.12% of the latter. Additionally, the former shows greater cycling stability and can last over 50 galvanostatic cycles, whereas the latter only lasts 16 cycles. EIS tests were further conducted on symmetric Zn||Zn cells by using Mn-CNFs and CNFs at temperatures from 30 °C to 70 °C. The results revealed that Mn-CNFs have a lower charge transfer resistance (R_{ct}) compared to the CNFs (Figure S2). This suggests that the incorporation of Mn ions effectively changes the solvation structure of the Zn ions, thereby enhancing the interfacial kinetics. To further analyze this phenomenon, an Arrhenius equation was used to determine the desolvation activation energy (E_a) of the Mn-CNFs and CNFs [27]. As presented in Figure 2c, the E_a of Mn-CNF is 11.91 $kJ{\cdot}mol^{-1}$, which is lower than that of CNF, which is 13.47 $kJ{\cdot}mol^{-1}$. This difference can be attributed to the effect of sieving for the desolvation process resulting in the modified channels within the Mn-CNF network [28].

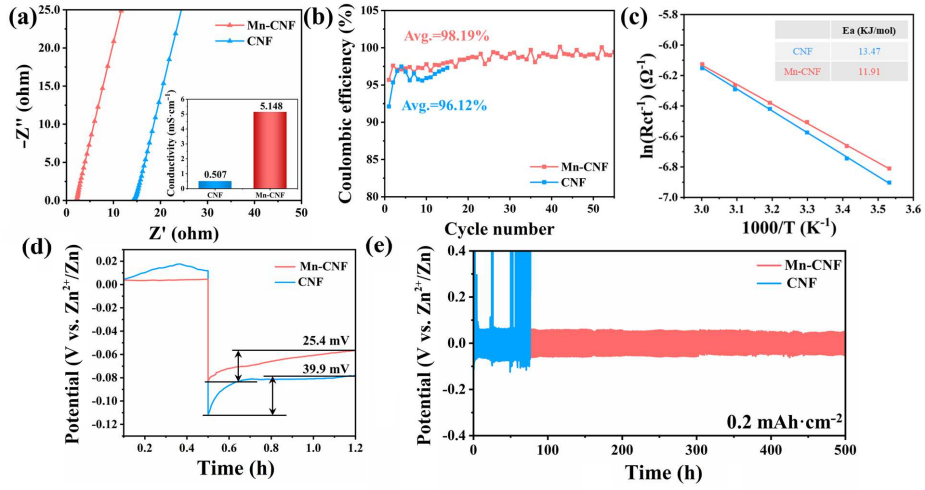

Figure 2. (**a**) Ionic conductivity of Mn-CNF and CNF; (**b**) Zn plating/stripping CEs with different separators at 1 $mA{\cdot}cm^{-2}$ and 1 $mAh{\cdot}cm^{-2}$; (**c**) Arrhenius curves and corresponding *Ea* values of Zn||Zn cells with Mn-CNF and CNF; (**d**) voltage–time curves of Zn plating processes with CNF and Mn-CNF separators at 0.2 $mAh{\cdot}cm^{-2}$; (**e**) galvanostatic cycling stability of symmetric Zn||Zn cells with Mn-CNFs and CNFs at 0.2 $mAh{\cdot}cm^{-2}$.

The voltage profiles of the galvanostatic plating conditions in the symmetric Zn||Zn cells that use Mn-CNFs and CNFs are illustrated in Figure 2d. The nucleation overpotential can be determined by the difference between the tip potential and the subsequent stable potential [29]. Notably, Mn-CNFs show a lower nucleation overpotential of 25.4 mV compared to the 39.9 mV of CNFs. This can be interpreted as a reduction in resistance during both the nucleation and growth phases for Mn-CNF, thereby significantly enhancing the quality of the Zn electroplating. Subsequently, the galvanostatic cycling stability of the symmetric Zn||Zn cells that use Mn-CNFs and CNFs is evaluated at a current density of 0.2 $mA \cdot cm^{-2}$ and a capacity limit of 0.2 $mAh \cdot cm^{-2}$, as depicted in Figure 2e. The cell that is integrated with Mn-CNFs as the separator shows the lowest overpotential of 50 mV and sustains a stable voltage profile over a duration of 500 h, after a brief initialization period of several galvanostatic cycles. Conversely, the cells that contain CNFs as the separator show a higher overpotential of approximately 80 mV and a substantially reduced operational lifespan, and cease to function effectively after only 70 h. The effectiveness of Mn-CNFs in moderating Zn nucleation and growth is the reason for the formation of a uniform and compact layer of Zn [30].

To gain further mechanistic insights, an XRD analysis was conducted on Zn anodes subjected to 20 galvanostatic cycles from the different batteries. Figure 3a shows the presence of $Zn_4SO_4(OH)_6 \cdot 4H_2O$ byproducts on the surface of the Zn electrode in the symmetric Zn||Zn cells that use CNFs with a corresponding large sheet-like byproducts observed via SEM [31]. The formation and detachment of the Zn dendrites are evident when using CNFs, which severely compromise cell performance (Figure 3b). In contrast, no discernible byproducts were detected on the Zn anode with Mn-CNFs as the separator, thus indicating a significant reduction in side effects. Additionally, the surface of the Zn anode is smooth without substantial Zn particles, which is attributed to the orderly regulation of the Zn-ion deposition facilitated by the Mn-CNFs (Figure 3c). The ultra-depth microscope images presented in Figure 3d further show that the Zn electrode with Mn-CNFs as the separator exhibits markedly less surface roughness compared to that with CNFs which confirms that Mn-CNFs can homogenize Zn deposited morphology by effectively regulating the Zn deposition behavior. Based on the aforementioned research, it is evident that the incorporation of Mn ions into the cellulose matrix effectively forms Mn-coordinated structures, thereby enhancing both the stability and ion conductivity (Figure 3e). This enhancement subsequently boosts the transport rate of the Zn ions [32,33]. Furthermore, the presence of Mn ions leads to a reduction in the nucleation overpotential for Zn, facilitating the uniform deposition of Zn ions and significantly reducing the risk of dendrite formation. Additionally, the abundant hydroxyl groups enhance both the solubility and diffusivity of Zn ions, thereby optimizing the cycling stability and rate in battery applications. It is also worth noting that the modified cellulose-based separator can achieve comparable electrochemical performance with other previously reported separators, especially in terms of cycle stability and ion conduction rates [34–36].

Zn||MnO_2 batteries were assembled to investigate the effectiveness of Mn-CNFs in enhancing the overall performance of the full batteries. For clarity, the Zn||MnO_2 batteries are referred to as the CNF and Mn-CNF batteries depending on whether the CNFs or Mn-CNFs are used. CV curves for the Zn||MnO_2 batteries with either CNFs or Mn-CNFs were plotted at a scan rate of 1 $mV \cdot s^{-1}$ (Figure 4a). The oxidation and reduction peak potentials of the Zn||MnO_2 batteries with CNFs were found to be 1.69 V and 1.34 V, respectively, which resulted in a potential difference of 0.35 V. The introduction of Mn-CNFs significantly increased the reduction potential, thus indicating a higher discharge voltage. Remarkably, the redox peak potential difference for the Zn||MnO_2 battery with Mn-CNFs was measured to be 0.35 V, which shows improved reversibility and rapid electrochemical reaction kinetics. In addition, the Mn-CNF battery showed exceptional cycling stability after over 1000 cycles at a current density of 1 $A \cdot g^{-1}$, which is a notable improvement compared to the CNF battery (Figure 4b). As shown in Figure 4c, the Mn-CNF battery shows significantly enhanced rate capabilities and retains a high discharge capacity of

95 mAh·g^{-1} at 2 A·g^{-1}. Most importantly, when the current density is reduced back to 0.2 A·g^{-1}, there is almost no decline in specific capacity, which shows its excellent recoverability. This enhanced rate performance can be attributed to the Mn-CNFs, which facilitate and homogenize Zn-ion transfer through the modified ion transport channels.

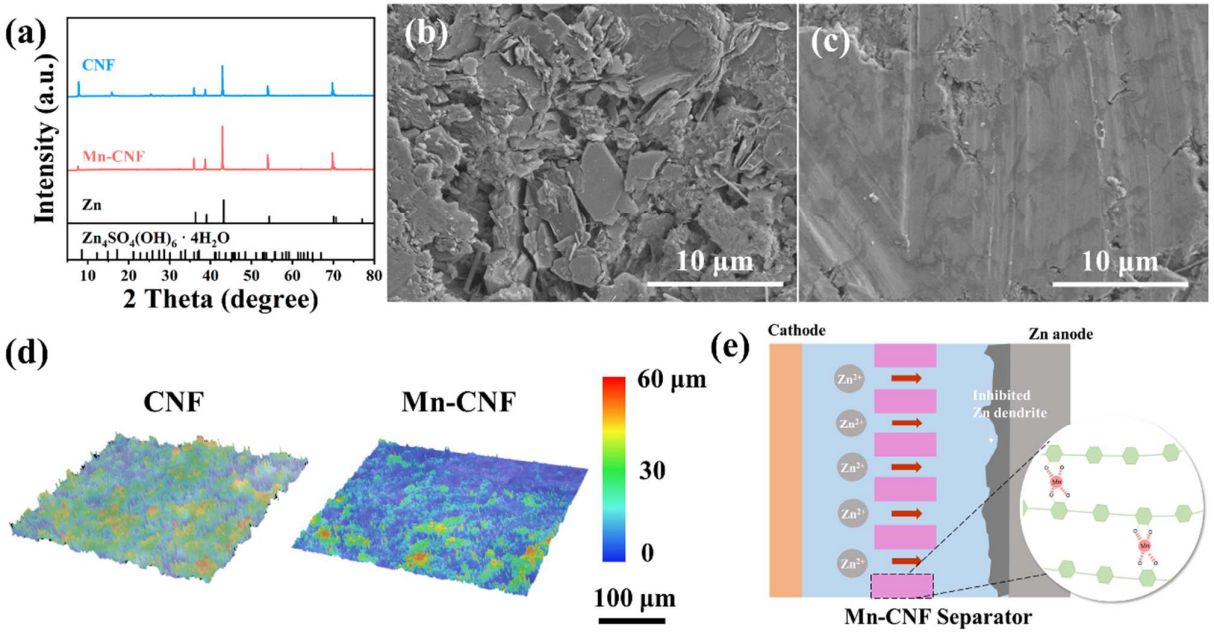

Figure 3. (**a**) XRD patterns of Zn anode in symmetric Zn||Zn cells which use Mn-CNFs and CNFs after 20 galvanostatic cycles. SEM images of Zn anode after being subjected to 20 galvanostatic cycles in symmetric Zn||Zn cells that use (**b**) CNFs and (**c**) Mn-CNFs, (**d**) three-dimensional depth distribution images of Zn anode in symmetric Zn||Zn cells that use Mn-CNFs and CNFs, and (**e**) proposed mechanism of Zn plating behavior in Mn-CNFs.

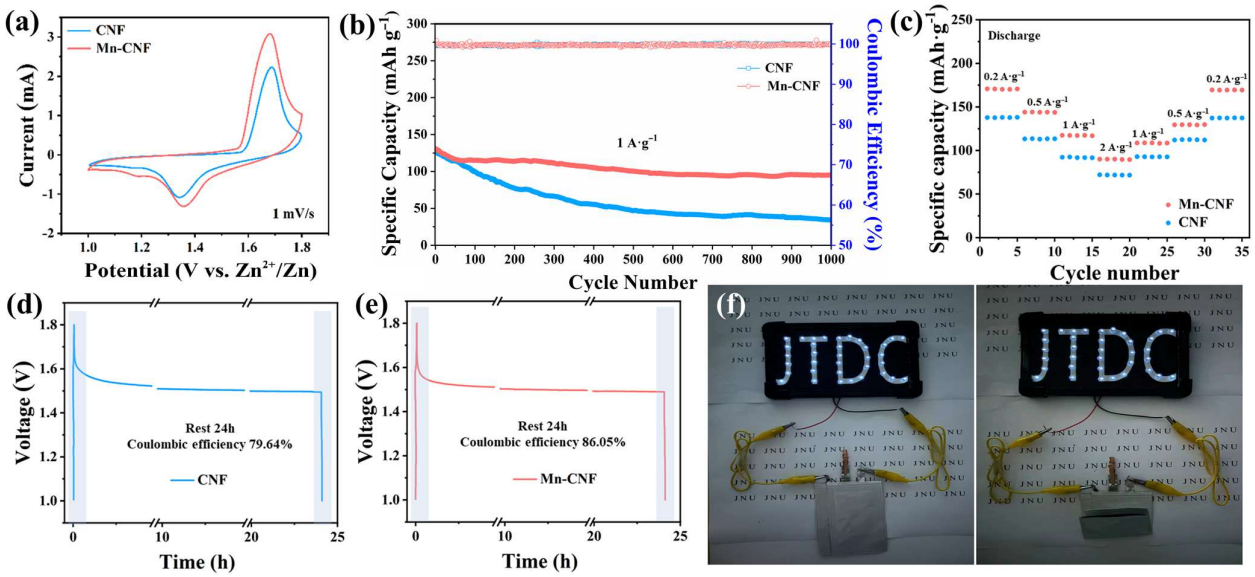

Figure 4. (**a**) CV curves of Zn||MnO_2 batteries with Mn-CNFs and CNFs at 1 mV·s^{-1}, (**b**) cycling performance at 1 A·g^{-1}, and (**c**) rate capability at different current densities. Self-discharge curves of Zn||MnO_2 batteries with (**d**) CNFs or (**e**) Mn-CNFs, and (**f**) flat and folded pouch cells light up LED display screen.

Furthermore, the Mn-CNF battery shows superior self-discharge resistance over the CNF battery as shown in Figure 4d,e. Compared to the CNF battery, the Mn-CNF battery maintains a CE of 86.05% after resting for 24 h, a slight improvement of 6.41% over the CNF battery. This enhanced self-discharge resistance indicates a reduction in side reactions, which positively contributes to the reversible capacity and energy density of AZIBs. Such improvements underscore the potential of Mn-CNFs as an effective separator that enhances the overall performance of AZIBs. To evaluate the practicality of Mn-CNFs, we assembled Zn||MnO_2 pouch cells that incorporate an Mn-CNF separator. Two of these pouch cells connected in a series can illuminate 35 LEDs that form the letters JDTC even when folded, which indicates that they have excellent flexibility for wearable applications (Figure 4f).

4. Conclusions

We have proposed a strategy to design a functional separator that is capable of high ionic conductivity through the structural expansion of interpolymer complexes and decoupling of Zn-ion transport from polymer chain relaxation. The Zn||MnO_2 battery, which uses Mn-CNFs as the separator, shows a significantly enhanced galvanostatic rate performance and cycling stability due to its ability to facilitate and optimize Zn-ion transport. This research highlights the effective modification of the crystalline structure of cellulose through Mn^{2+} coordination with CNFs, which reinforces the inner ion transfer channel and increases Zn-ion movement. The presence of a large number of oxygen functional groups in cellulose further contributes to this process, thus allowing for Zn-ion transport that is independent of polymer chain motion. The findings provide valuable insights for the development of efficient and reliable separators for advanced electrochemical energy storage systems.

Supplementary Materials: The following supporting information can be downloaded at: https://www.mdpi.com/article/10.3390/batteries10120416/s1. Figure S1: Zeta potentials of Mn-CNF and CNF separators; Figure S2: Nyquist plots of the symmetric Zn||Zn cells utilizing (a) Mn-CNF and (b) CNF separators at different temperatures.

Author Contributions: Conceptualization, J.C. and H.J.; methodology, J.C.; formal analysis, J.C. and K.W.; investigation, J.C., K.W. and X.N.; data curation, K.W.; writing—original draft preparation, J.C.; writing—review and editing, H.J., B.T. and S.J.; visualization, K.W.; supervision, B.T. and J.Z.; project administration, B.T.; funding acquisition, H.J. and S.J. All authors have read and agreed to the published version of the manuscript.

Funding: This research was funded by the Opening Project of the Key Laboratory of Clean Dyeing and Finishing Technology of Zhejiang Province (QJRZ2206) and the Research Centre of Textiles for Future Fashion (P0049572).

Data Availability Statement: Data will be made available on request. The data are not publicly available due to privacy.

Conflicts of Interest: The authors declare no conflicts of interest.

References

1. Zhang, C.; Shen, L.; Shen, J.; Liu, F.; Chen, G.; Tao, R.; Ma, S.; Peng, Y.; Lu, Y. Anion-sorbent composite separators for high-rate lithium-ion batteries. *Adv. Mater.* **2019**, *31*, 1808338. [CrossRef] [PubMed]
2. Tang, C.; Yu, L.; Jiang, Q.; Gu, R.; Zhang, Y.; Liu, Z.; Cai, W.; Wu, H.; Zhang, Y.; Yao, M. Polymer-based electrolyte for lithium-based high-energy-density and safe energy storages devices: Strategy and mechanisms. *Renewables* **2024**, *2*, 297–340. [CrossRef]
3. Zheng, J.; Zhao, Q.; Tang, T.; Yin, J.; Quilty, C.; Renderos, G.; Liu, X.; Deng, Y.; Wang, L.; Bock, D. Reversible epitaxial electrodeposition of metals in battery anodes. *Science* **2019**, *366*, 645–648. [CrossRef]
4. Chang, N.; Li, T.; Li, R.; Wang, S.; Yin, Y.; Zhang, H.; Li, X. An aqueous hybrid electrolyte for low-temperature zinc-based energy storage devices. *Energy Environ. Sci.* **2020**, *13*, 3527–3535. [CrossRef]
5. Fan, K.; Tsang, Y.; Huang, H. Computational design of promising 2D electrode materials for Li-ion and Li-S battery applications. *Mater. Rep. Energy* **2023**, *3*, 100213. [CrossRef]
6. Zhou, C.; Wang, H.; Li, Q.; Wu, F.; Cao, S.; Li, J.; Tan, Z. An Ag/C core-shell composite functionalized carbon nanofiber film as freestanding bifunctional host for advanced lithium-sulfur batteries. *Adv. Fiber Mater.* **2024**, *6*, 181–194. [CrossRef]

7. Jia, H.; Liu, K.; Lam, Y.; Tawiah, B.; Xin, J.; Nie, W.; Jiang, S. Fiber-based materials for aqueous zinc ion batteries. *Adv. Fiber Mater.* **2023**, *5*, 36–58. [CrossRef]
8. Zou, Y.; Liu, T.; Du, Q.; Li, Y.; Yi, H.; Zhou, X.; Li, Z.; Gao, L.; Zhang, L.; Liang, X. A four-electron Zn-I_2 aqueous battery enabled by reversible $I^-/I_2/I^+$ conversion. *Nat. Commun.* **2021**, *12*, 170. [CrossRef] [PubMed]
9. Jia, H.; Qiu, M.; Tang, C.; Liu, H.; Xu, J.; Tawiah, B.; Jiang, S.; Zhang, X. Advanced flexible carbon-based current collector for zinc storage. *Adv. Fiber Mater.* **2022**, *4*, 1500–1510. [CrossRef]
10. Zhang, M.; Gong, Y.; Liu, Y.; Liu, Y.; Huang, S.; Niu, Z.; Zhang, X.; Zhang, X.; Cao, D. Carbon nanofibers encapsulated CoNiFe bifunctional electrocatalysts for durable Zn-air batteries at room and −40 °C ultralow temperatures. *Renewables* **2024**, *2*, 353–363. [CrossRef]
11. Wang, Y.; Li, N.; Liu, H.; Shi, J.; Li, Y.; Wu, X.; Wang, Z.; Huang, C.; Chen, K.; Zhang, D. "Zincophilic-hydrophobic" PAN/PMMA nanofiber membrane toward high-rate dendrite-free Zn anode. *Adv. Fiber Mater.* **2023**, *5*, 2002–2015. [CrossRef]
12. Yu, Y.; Liu, M.; Chen, Z.; Zhang, Z.; Qiu, T.; Hu, Z.; Xiang, H.; Zhu, L.; Xu, G.; Zhu, M. Advances in nonwoven-based separators for lithium-ion batteries. *Adv. Fiber Mater.* **2023**, *5*, 1827–1851. [CrossRef]
13. Chen, Y.; Li, S.; Li, X.; Mei, C.; Zheng, J.; E, S.; Duan, G.; Liu, K.; Jiang, S. Liquid transport and real-time dye purification via lotus petiole-inspired long-range-ordered anisotropic cellulose nanofibril aerogels. *ACS Nano* **2021**, *15*, 20666–20677. [CrossRef] [PubMed]
14. Zhongjie, Y.; Shijie, D.; Weihao, L.; Zhenzhen, Z.; Xinmin, H.; Lingling, M. Preparation and properties of nanocellulose-enhanced dua lnetwork-mediated hydrogels. *Basic Sci. J. Text. Univ.* **2022**, *35*, 16–22.
15. Fu, H.; Wang, B.; Li, J.; Xu, J.; Li, J.; Zeng, J.; Gao, W.; Chen, K. A self-healing, recyclable and conductive gelatin/nanofibrillated cellulose/Fe^{3+} hydrogel based on multi-dynamic interactions for a multifunctional strain sensor. *Mater. Horiz.* **2022**, *9*, 1412–1421. [CrossRef] [PubMed]
16. Chen, D.; Zhao, X.; Wei, X.; Zhang, J.; Wang, D.; Lu, H.; Jia, P. Ultrastretchable, tough, antifreezing, and conductive cellulose hydrogel for wearable strain sensor. *ACS Appl. Mater. Interfaces* **2020**, *12*, 53247–53256. [CrossRef]
17. Yang, C.; Wu, Q.; Xie, W.; Zhang, X.; Brozena, A.; Zheng, J.; Garaga, M.N.; Ko, B.H.; Mao, Y.; He, S.; et al. Copper-coordinated cellulose ion conductors for solid-state batteries. *Nature* **2021**, *598*, 590–596. [CrossRef]
18. Qian, J.; Dong, Q.; Chun, K.; Zhu, D.; Zhang, X.; Mao, Y.; Culver, J.N.; Tai, S.; German, J.R.; Dean, D.P.; et al. Highly stable, antiviral, antibacterial cotton textiles via molecular engineering. *Nat. Nanotechnol.* **2023**, *18*, 168–176. [CrossRef]
19. Zhou, W.; Chen, M.; Tian, Q.; Chen, J.; Xu, X.; Wong, C. Cotton-derived cellulose film as a dendrite-inhibiting separator to stabilize the zinc metal anode of aqueous zinc ion batteries. *Energy Storage Mater.* **2022**, *44*, 57–65. [CrossRef]
20. Yang, S.; Zhang, Y.; Zhang, Y.; Deng, J.; Chen, N.; Xie, S.; Ma, Y.; Wang, Z. Designing anti-swelling nanocellulose separators with stable and fast Ion transport channels for efficient aqueous zinc-ion batteries. *Adv. Funct. Mater.* **2023**, *33*, 2304280. [CrossRef]
21. Cao, J.; Zhang, D.; Gu, C.; Zhang, X.; Okhawilai, M.; Wang, S.; Han, J.; Qin, J.; Huang, Y. Modulating Zn deposition via ceramic-cellulose separator with interfacial polarization effect for durable zinc anode. *Nano Energy* **2021**, *89*, 106322. [CrossRef]
22. Woottapanit, P.; Yang, C.; Cao, J.; Limphirat, W.; Saneewons na ayuttaya, S.; Zhang, X.; Wangyao, P.; Qin, J. Inhibition of zinc dendrite growth by WC-cellulose separators for high-performance zinc-ion batteries. *ACS Appl. Energy Mater.* **2023**, *6*, 10578–10584. [CrossRef]
23. Qiu, M.; Liu, H.; Luo, J.; Tawiah, B.; Fu, S.; Jia, H. Long-life zinc electrodes achieved by oxygen plasma functionalization. *Chem. Commun.* **2022**, *58*, 993–996. [CrossRef] [PubMed]
24. Zhang, H.; Li, S.; Xu, L.; Momen, R.; Deng, W.; Hu, J.; Zou, G.; Hou, H.; Ji, X. High-yield carbon dots interlayer for ultra-stable zinc batteries. *Adv. Energy Mater.* **2022**, *12*, 2200665. [CrossRef]
25. Li, R.; Wei, J.; Xu, S.; Zhu, Q.; Liu, W.; Qiu, Y.; Jiang, Q. Full-degradable composites reinforced by the low temperature treated cotton fabrics with enhanced strength and interfacial bonding. *Compos. Part B* **2019**, *177*, 107269. [CrossRef]
26. Li, Z.; Ye, L.; Zhou, G.; Xu, W.; Zhao, K.; Zhang, X.; Hong, S.; Ma, T.; Li, M.; Liu, C. A water-gating and zinc-sieving lignocellulose nanofiber separator for dendrite-free rechargeable aqueous zinc ion battery. *Chem. Eng. J.* **2023**, *457*, 141160. [CrossRef]
27. Zhang, L.; Huang, J.; Guo, H.; Ge, L.; Tian, Z.; Zhang, M.; Wang, J.; He, G.; Liu, T.; Hofkens, J. Tuning ion transport at the anode-electrolyte Interface via a sulfonate-rich ion-exchange layer for durable zinc-iodine batteries. *Adv. Energy Mater.* **2023**, *13*, 2203790. [CrossRef]
28. Lin, P.; Cong, J.; Li, J.; Zhang, M.; Lai, P.; Zeng, J.; Yang, Y.; Zhao, J. Achieving ultra-long lifespan Zn metal anodes by manipulating desolvation effect and Zn deposition orientation in a multiple cross-linked hydrogel electrolyte. *Energy Storage Mater.* **2022**, *49*, 172–180. [CrossRef]
29. Liang, P.; Yi, J.; Liu, X.; Wu, K.; Wang, Z.; Cui, J.; Liu, Y.; Wang, Y.; Xia, Y.; Zhang, J. Highly reversible Zn anode enabled by controllable formation of nucleation sites for Zn-based batteries. *Adv. Funct. Mater.* **2020**, *30*, 1908528. [CrossRef]
30. Liu, P.; Zhang, Z.; Hao, R.; Huang, Y.; Liu, W.; Tan, Y.; Li, P.; Yan, J.; Liu, K. Ultra-highly stable zinc metal anode via 3D-printed g-C_3N_4 modulating interface for long life energy storage systems. *Chem. Eng. J.* **2021**, *403*, 126425. [CrossRef]
31. Liu, Z.; Wang, R.; Ma, Q.; Wan, J.; Zhang, S.; Zhang, L.; Li, H.; Luo, Q.; Wu, J.; Zhou, T. A dual-functional organic electrolyte additive with regulating suitable overpotential for building highly reversible aqueous zinc ion batteries. *Adv. Funct. Mater.* **2023**, *34*, 2214538. [CrossRef]
32. Dong, Q.; Zhang, X.; Qian, J.; He, S.; Mao, Y.; Brozena, A.H.; Zhang, Y.; Pollard, T.P.; Borodin, O.A.; Wang, Y.; et al. A cellulose-derived supramolecule for fast ion transport. *Sci. Adv.* **2022**, *8*, eadd2031. [CrossRef] [PubMed]

33. Zhang, X.F.; Ma, X.; Hou, T.; Guo, K.; Yin, J.; Wang, Z.; Shu, L.; He, M.; Yao, J. Inorganic salts induce thermally reversible and anti-freezing cellulose hydrogels. *Angew. Chem. Int. Ed.* **2019**, *58*, 7366–7370. [CrossRef] [PubMed]
34. Zong, Y.; He, H.; Wang, Y.; Wu, M.; Ren, X.; Bai, Z.; Wang, N.; Ning, X.; Dou, S. Functionalized separator strategies toward advanced aqueous zinc-ion batteries. *Adv. Energy Mater.* **2023**, *13*, 2300403. [CrossRef]
35. Du, H.; Yi, Z.; Li, H.; Lv, W.; Hu, N.; Zhang, X.; Chen, W.; Wei, Z.; Shen, F.; He, H. Separator design strategies to advance rechargeable aqueous zinc ion batteries. *Chem. Eur. J.* **2024**, *30*, e202303461. [CrossRef]
36. Kim, J.; Gu, M.; Lee, D.; Kim, J.; Oh, Y.; Min, S.; Kim, B.; Lee, S. Functionalized nanocellulose-integrated heterolayered nanomats toward smart battery separators. *Nano Lett.* **2016**, *16*, 5533–5541. [CrossRef]